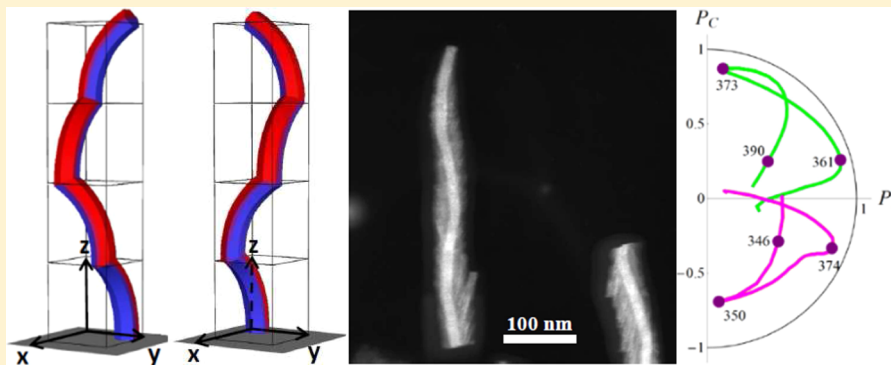


Curved-Lattice Epitaxial Growth of $\text{In}_x\text{Al}_{1-x}\text{N}$ Nanospirals with Tailored Chirality

Ching-Lien Hsiao,* Roger Magnusson, Justinas Palisaitis, Per Sandström, Per O. Å. Persson, Sergiy Valyukh, Lars Hultman, Kenneth Järrendahl, and Jens Birch

Department of Physics, Chemistry, and Biology (IFM), Linköping University, S81 83 Linköping, Sweden

S Supporting Information



ABSTRACT: Chirality, tailored by external morphology and internal composition, has been realized by controlled curved-lattice epitaxial growth of $\text{In}_x\text{Al}_{1-x}\text{N}$ nanospirals. The curved morphology of the spiral segments is a result of a lateral compositional gradient while maintaining a preferred crystallographic growth direction, implying a lateral gradient in optical properties. Individual nanospirals show an asymmetric core–shell structure with curved basal planes. Mueller matrix spectroscopic ellipsometry shows that the tailored chirality is manifested in the polarization state of light reflected off the nanospirals.

KEYWORDS: *InAlN, nanospirals, chirality, sputtering, CLEG, GLAD*

Iridescent structural colors and polarization properties of the light shown in the reflection from insects, such as butterflies and scarab beetles, attract attention to explore the relationship between the microstructures and their optical behaviors.^{1–6} One of the most intriguing phenomena is that some beetles reflect light with a very high degree of circular polarization (P_c).⁴ This transformation of unpolarized incident light into nearly circularly polarized light is associated with a chiral stacking of chitin-based layers, showing a helicoidal structure, in the cuticle.^{3–6} By mimicking these natural helicoidal structures, it is possible to manipulate optical polarization states. In addition, further insight into the origin of natural polarization can be gained.

Chirality in various materials, for instance, Au helices and related chiral metallic structures,^{7–10} cholesteric liquid crystals (CLCs),¹¹ and sculpted thin films,^{12–14} including dielectric oxide and fluoride nanostructures, polymers,¹⁵ and hybrid nematic liquid crystals imposed in inorganic nanostructures,¹⁶ have been used to develop circular polarization sensitive optical elements, such as broadband circular polarizers and wavelength-tunable polarizers or filters.^{7–12} Mostly, these chiral materials are tailored by external morphology. The optical chirality in the materials are often due to either circular dichroism in chiral metallic materials^{7–9} or optical Bragg reflection from birefringent dielectrics.^{12–15} Recently, hybrid nanocolloids^{17,18}

and composite metal nanohelices related chiral plasmonic structures^{19,20} have been demonstrated to enhance the chiral-optical response in the visible range utilizing surface plasmon resonance of metal nanoparticles.

Approaches to make inorganic chiral materials are mainly based on three-dimensional (3D) lithography^{7–10,21} and/or glancing angle deposition (GLAD)^{13,22–24} to tailor the structural chirality. However, 3D lithography is a complicated and tedious process while GLAD often provides amorphous or polycrystalline structures, frequently with a broadening of the spiral and rod diameters with increasing growth time. Such broadening may destroy the nanostructures due to structural coalescence at long-time growth. In addition, none of the approaches are suitable for making internal lateral compositional gradients in the nanostructures.

In a previous study,²⁵ we have demonstrated a unique growth mechanism, here denoted controlled curved-lattice epitaxial growth (CLEG), for making one-axis curved $\text{In}_x\text{Al}_{1-x}\text{N}$ nanocrystals having a graded single-crystalline structure and a stress/strain free curved lattice. In this Letter, we show how this kind of nanocrystals can be used to tailor chirality by utilizing

Received: September 16, 2014

Revised: November 14, 2014

Published: November 26, 2014

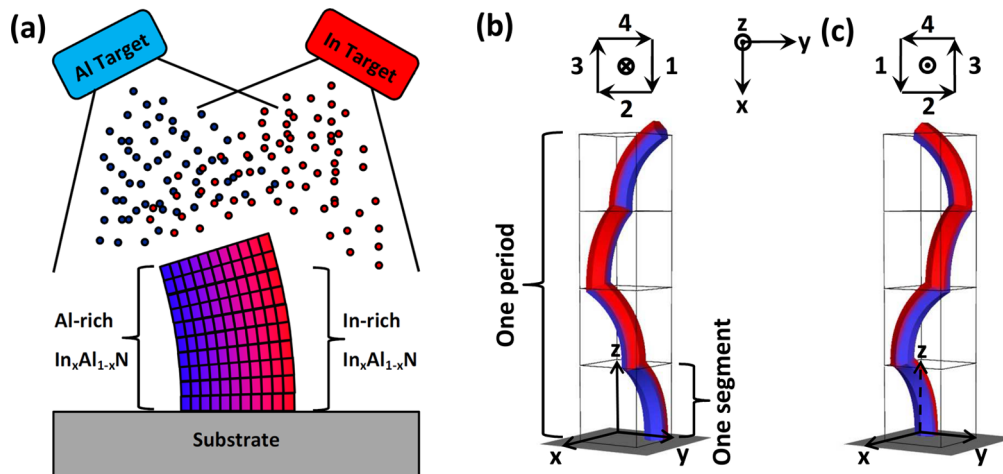


Figure 1. Schematic illustration of CLEG and the growth of one period of a nanospiral structure. (a) A curved rod segment of an $\text{In}_x\text{Al}_{1-x}\text{N}$ nanospiral (one-fourth of a spiral turn in this sample) controlled by CLEG. Blue to red color gradient along the lateral direction of the curved rod segment indicates the compositional gradient from high to low Al content $\text{In}_x\text{Al}_{1-x}\text{N}$. (b,c) One period of a left- and right-handed nanospiral structure, respectively. One turn of a nanospiral is comprised of four curved rod segments, obtained by temporal control of the azimuthal orientation of the deposition fluxes. The arrow diagrams illustrate the sequence and direction of curvature of each segment, as seen from the top, in the two cases of left- and right-handed nanospiral growth.

the material's intrinsic anisotropic properties. In contrast to other literature reports,^{13,14,22–24} our material has a chirality manifested not only by the spiral morphology but also by an internal chemical and structural gradient. To achieve this we have developed a process for making single-crystalline $\text{In}_x\text{Al}_{1-x}\text{N}$ nanospirals using CLEG. No obvious broadening of the spiral and rod diameters along the growth direction is observed. The curved lattice and lateral compositional gradient in the nanospirals are characterized by lattice-resolved images, (scanning) transmission electron microscopy ((S)TEM), energy-dispersive X-ray spectroscopy (EDX), and valence electron-energy loss spectroscopy (VEELS). The unique CLEG $\text{In}_x\text{Al}_{1-x}\text{N}$ nanospirals are also transparent, making the films suitable for optical applications. The possibility to tailor the degrees of linear and circular polarizations (including the handedness) of light reflected off surfaces covered by specifically designed $\text{In}_x\text{Al}_{1-x}\text{N}$ nanospirals is demonstrated in the ultraviolet-visible (UV-vis) region, suggesting that the CLEG $\text{In}_x\text{Al}_{1-x}\text{N}$ nanospirals can be important in high-performance optical components.

The concept of the CLEG nanospiral growth method is outlined in Figure 1. On the basis of the original report by Radnócz et al., Figure 1 illustrates the concept of how a curved segment of an $\text{In}_x\text{Al}_{1-x}\text{N}$ nanospiral with an ideally lateral compositional gradient can be grown by the CLEG technique when the substrate is kept stationary.²⁵ Blue to red color gradient along the lateral direction of the rod indicates the intrarod compositional gradient from high to low Al content in the $\text{In}_x\text{Al}_{1-x}\text{N}$. Because of the lateral lattice parameter gradient between the Al- and In-rich sides of the $\text{In}_x\text{Al}_{1-x}\text{N}$ crystallite the rod becomes curved. Hence, a curved nanorod is single crystalline but with a laterally graded composition. Thus, based on a wurtzite crystal structure with a preferred nanorod growth along the crystallographic *c*-axis, the crystal structure of the nanorods can be described as basal planes with laterally changing internal lattice spacings *a* and a corresponding lateral variation in the *c* lattice-spacing. With temporal control of the substrate azimuthal orientation, nanospirals can be formed by, for example, sequentially stacking segments of curved nanorod

segments on top of each other, where each segment is incrementally rotated around the spiral axis. By controlling the growth rate, segment length, rotation direction, and incremental rotation angle, spirals are tailored to predetermined handedness, pitch, and height. Figure 1b,c shows schematic drawings of the first period of such right-handed and left-handed nanospirals, respectively, each comprised of four arched rod segments to complete one turn in a nanospiral. Subsequent replication of these first segments then forms multiple-turn nanospirals. The internal lateral composition gradient makes it possible to tailor the chirality of the CLEG nanospirals combining two effects: (1) a chirality due to the external spiral morphology [Figure 1b,c] and (2) a chirality from precession of the anisotropic optical properties, most importantly due to the lateral gradient in composition and lattice parameter [Figure 1a] but also in part due to that $\text{In}_x\text{Al}_{1-x}\text{N}$ have a uniaxial wurtzite structure.^{26–30} The second effect has profound influence on the optical response of the system due to the rotation of a birefringent and dichroic structure. Hence, the CLEG $\text{In}_x\text{Al}_{1-x}\text{N}$ nanospirals are unique in the sense that the chirality is manifested not only by the external spiral morphology but also by the internal rotation of the crystalline structure, which will give a strong interaction with light.^{31,32}

The $\text{In}_x\text{Al}_{1-x}\text{N}$ nanostructure growth was performed in an ultrahigh-vacuum (UHV) magnetron sputter epitaxy (MSE) system evacuated to a base pressure of $<3 \times 10^{-9}$ Torr (4×10^{-7} Pa). Four sputter sources were symmetrically positioned in the chamber base directed toward the substrate at their common focal point, giving a 30° angle of incidence of the deposition fluxes. All target-to-substrate distances were around 13 cm. More details of the growth system can be found elsewhere.^{27–30} The *c*-plane sapphire substrates, $1 \times 1 \text{ cm}^2$, were degreased in subsequent ultrasonic baths of trichloroethylene, acetone, and isopropanol for 5 min each and then blown dry with pure nitrogen. Prior to the $\text{In}_x\text{Al}_{1-x}\text{N}$ nanostructure, nanospiral, or nanorod growth, the sapphire substrates were outgassed for 30 min at 1000°C . Then, an epitaxial ~ 30 nm 111-oriented VN seed layer was deposited at 850°C by reactive sputtering from a vanadium target.

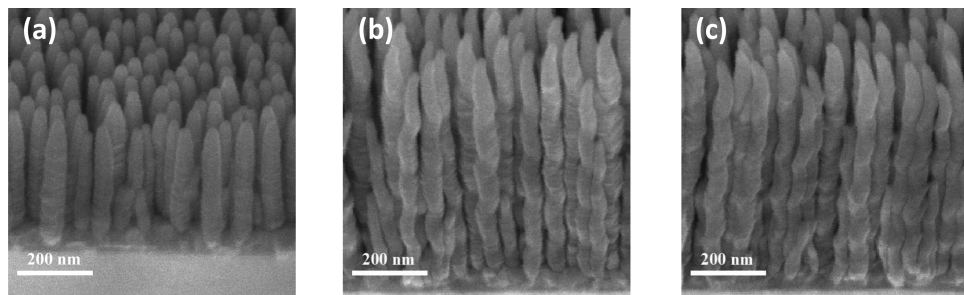


Figure 2. SEM images of $\text{In}_x\text{Al}_{1-x}\text{N}$ nanorods and nanospirals. (a) Straight nanorods. (b,c) Left- and right-handed nanospirals, respectively, comprising 5 turns at 200 nm pitch. The nanospiral's growth is homogeneous in both length ($\sim 1 \mu\text{m}$) and diameter (60 nm).

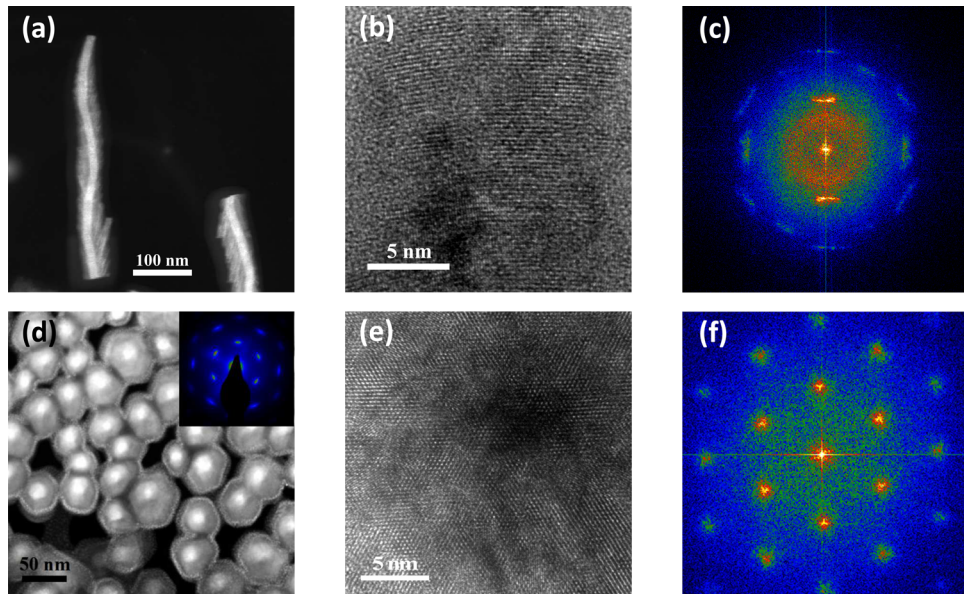


Figure 3. STEM and lattice-resolved images, and SAED and FFT patterns of $\text{In}_x\text{Al}_{1-x}\text{N}$ nanospirals. (a) Side-view STEM image of free-standing nanospirals with curved rod structure and bright core (darker shell). (b) Lattice-resolved image of curved lattice taken from the core at the nanospiral top. (c) Corresponding FFT from (b) with $\sim 25^\circ$ wide arcs around 0002 and 01\bar{1}0 attributed to the curved lattice. (d) Top-view STEM image with corresponding SAED pattern revealing bright and dark areas in all hexagonal cross-sections along the growth direction. (e) A lattice-resolved image with hexagonal lattices in both core (dark) and shell (bright). (f) Corresponding FFT pattern from (e) exhibiting a well-defined hexagonal spotty pattern.

$\text{In}_x\text{Al}_{1-x}\text{N}$ nanostructures were grown at 600 °C by reactive cosputtering from Al (99.999%) and In (99.999%) targets. The Al and In magnetron powers were fixed at 300 and 10 W, respectively. All the sputtering processes were carried out in a pure nitrogen (99.999999%) atmosphere at a working pressure of 5 mTorr. Straight $\text{In}_x\text{Al}_{1-x}\text{N}$ nanorods were first grown by the MSE using a constant substrate rotation of 40 rpm. The obtained growth rate, $\sim 0.178 \text{ nm/s}$, was used to determine the nanospiral growth conditions. The growth of left- and right-handed nanospirals were then implemented by temporal control of the substrate azimuthal orientations in steps of 90°. The nanospirals were designed having five complete turns with a period of 200 nm, giving a total length of 1 μm . Each period of the spiral were comprised by four 50 nm curved segments, sequentially stacked and mutually rotated, on top of each other, as shown in Figure 1b,c. The growth time of each segment was 281 s. The incremental rotation angles were -90° and 90°, as seen from source, for growing left- and right-handed nanospirals, respectively.

The morphology of as-grown samples was characterized by a LEO-1550 field-emission scanning electron microscope (FE-SEM) in which the sample holder is capable of 360° rotation

and 75° tilt. Figure 2 shows SEM side-view images of both straight nanorods and nanospirals grown by MSE. Figure 2a shows straight $\text{In}_x\text{Al}_{1-x}\text{N}$ nanorods, which are well separated and have a uniform height of $\sim 640 \text{ nm}$. The distribution of the rods is homogeneous throughout the sample. All nanorods exhibit a tapered top and stepped side surface, which is attributed to the formation of a core–shell nanorod structure according to our previous study.²⁷ Figure 2b,c demonstrate left- and right-handed nanospirals comprised of 5 turns with a period of 200 nm. The nanospirals are seen to be rather homogeneous in height ($\sim 1 \mu\text{m}$), spiral diameter ($\sim 80 \text{ nm}$), and rod diameter ($\sim 60 \text{ nm}$). Morphologically, except for the spiral shape, the nanospirals feature the same properties as the straight nanorods by virtue of the high stability and controllability of MSE. Moreover, no broadening is observed toward the top of the nanorods and nanospirals, which is an essential difference to spirals grown by conventional GLAD.^{22–24}

Analyses of microstructural properties and compositional mappings were performed using (S)TEM, EDX, and VEEELS. Side-view (S)TEM analyses of individual $\text{In}_x\text{Al}_{1-x}\text{N}$ nanospirals, dispersed on amorphous carbon films suspended on Cu-grids,

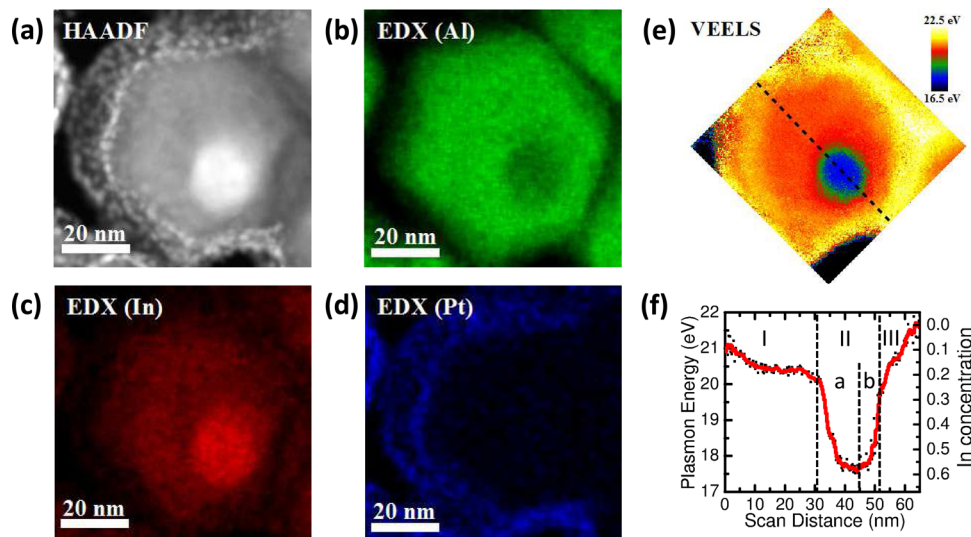


Figure 4. Composition and plasmon energy analyses of a single $\text{In}_x\text{Al}_{1-x}\text{N}$ nanospiral. (a) Top-view STEM (HAADF) image with bright (high mass) core and dark (low mass) shell in a hexagonal nanospiral cross-section along the growth direction showing a non-concentric core–shell structure. (b–d) Corresponding EDX maps of Al (b), In (c), and Pt (d) revealing higher In (Al) content in the core (shell), excluding the existence of In on the most outer shell (brighter spots). (e,f) VEELS map I and extracted line profile of plasmon energy (f) from the map (in e) exhibiting a small compositional gradient from left shell (I) and large compositional gradients in the asymmetric core (II-a,b) and right shell (III).

were investigated by using a FEI Tecnai G² TF-20 UT FEG microscope operated at 200 kV.^{33,34} Nanometer-scale analytical EDX and VEELS mapping of nanospiral cross sections, as seen in top-view projection, prepared by using a Carl Zeiss Crossbeam 1540 EsB focused ion beam milling instrument, were performed by using the double corrected Linköping Titan³ 60–300 operated at 300 kV, equipped with a large solid angle Super-X EDX detector and high-speed Gatan Imaging Filter Quantum ERS spectrometers.

Figure 3 shows nanostructural analyses of the nanospirals in both side-view and top-view projections. Figure 3a is a mass-contrast STEM image of free nanospirals. The micrograph shows well-defined spiral nanorods with a brighter core and a darker shell due to higher In and Al contents in the core and shell, respectively. In addition, the shell exhibits sprouts on the core, predominantly on its concave side and inclined with respect to the core direction, corresponding to the stepped side surfaces, seen in Figure 2. A lattice-resolved side-view image taken of the core at the tapered top of a nanospiral is shown in Figure 3b. A curved lattice is clearly observed. Figure 3c shows the corresponding fast Fourier transform (FFT) exhibiting semiarcs corresponding to the curved lattice. Examining the FFT, using the center of the arcs, a hexagonal structure can be determined with the average *c*-axis along the growth direction of the spiral axis, the zone axis being along [01 $\bar{1}$ 0] (see Supporting Information S1). A top-view STEM image of the nanospirals, showing their cross sections at an arbitrary position, is shown in Figure 3d. All spirals exhibit hexagonal cross sections with a non-concentric core–shell structure where cores are displaced toward the outside of the nanospirals, as deduced by comparing Figure 3, panels a and d. The ensemble nanospirals across the 1 cm² substrates show high in-plane ordering with respect to shape, crystalline orientation, and direction of compositional gradient. The inset of Figure 3d shows a corresponding selective-area electron diffraction (SAED) pattern of the spirals. A hexagonal pattern formed with semiarcs implies a [0001] zone axis and a slight spread in azimuthal orientation of the nanospirals. Extracting the radial

intensity line profiles across two of the arc's centers (see Supporting Information S2) yielded asymmetric peaks with long tails toward the center, confirming that a lateral gradient of lattice constant in the spirals exists. A top-view lattice-resolved image taken at the core area of a nanospiral, shown in Figure 3e, presents its crystalline hexagonal lattice with gradient dark/bright contrast from the core to the edge shell. A corresponding FFT of the lattice as seen in the top-view, shown in Figure 3f, exhibits a well-defined hexagonal pattern, in contrast to top-view SAED pattern (inset of Figure 3d) obtained from multiple cross sections of nanospirals. It indicates that the semi arcs in the SAED pattern are due to slight twist misorientations between the nanospirals. This can be explained by the rotating lattice inside each nanospiral, which in general will occur due to the combination of curved lattice planes and the precession of the *c*-axis along the spirals.

To explore the composition in the nanospirals EDX spectroscopy and VEELS^{27,33,34} were employed using a nanoprobe to map a cross section of a single nanospiral. Figure 4a shows a higher magnification top-view STEM image of a nanospiral, revealing that the core of the nanospiral has a hexagonal cross section with the same in-plane orientation as the outer shell although this is an asymmetrical core–shell structure. The In-rich core is around 20 nm thick and surrounded by an Al-rich shell with a thickness asymmetry spiraling along the core. Figure 4b–d shows corresponding EDX elemental maps of Al, In, and Pt from the same area. The maps are converted from EDX spectrum images using the integrated intensity of the Al-K, In-L, and Pt-L lines, respectively. Typical spectra acquired at the core center, shell, and edge of the shell are shown in Supporting Information S3. As can be seen, the core and shell have complementary contrast for the Al and In maps, which proves that the nanospirals have higher In concentration at the core than in the shell and vice versa for Al as induced by the mass-contrast STEM image of Figure 4a. The Pt map shows that the brighter spots presented on the outer shell in the STEM image are Pt and hence is an artifact from the focused ion beam sample preparation

procedure. To quantify the variation of the InN mole fraction in the nanospiral a VEELS map was acquired of the entire spiral cross-section. Figure 4e shows the map comprised of the peak energy of the bulk plasmon, which is strongly correlated to the group-III nitride compound composition.^{37,34} A line profile extracted from the VEELS map, indicated as the dashed line in Figure 4e, is shown in Figure 4f and clearly demonstrates the asymmetric composition profile across the cross-section of the spiral. The corresponding InN mole fraction was calculated from the plasmon energy and is shown by the right vertical axis. It can be divided into four zones: In zone I (shell on the left, ~30 nm), the InN mole fraction, x , shows a gradual increase from 0.05 to 0.20, then follows a sharp increase to $x = 0.58$ in zone II-a (left-hand side of core, ~15 nm) and decreases dramatically again to $x = 0.25$ in zone II-b (right-hand side of core, ~7 nm), and finally decreases from 0.25 to almost $x = 0$ in the zone III (shell on the right, ~13 nm).

Formation of core–shell structures are often shown in ternary III-nitrides^{27,35,36} due to spinodal decomposition^{29,30} and a low InN decomposition temperature of 550 °C.³⁷ The phase separation can easily happen when the alloy composition is in the miscibility gap of $\text{In}_x\text{Al}_{1-x}\text{N}$, $0.1 < x < 0.9$.^{26,29,30} When the growth temperature is in the equilibrium condition, a concentric core–shell structure with a more distinct two-phase compositions can be formed due to the higher adatom mobility and high In desorption rate on the sidewalls.^{35,36} The spiraling asymmetric core–shell structure with graded lateral composition supports that the growth is controlled in the non-equilibrium region. It should be stressed that the nanospirals in this work are primarily formed thanks to the lateral compositional gradients in the cores, as shown by the TEM analyses, and not so much due to the spiraling asymmetric shell. The CLEG phenomenon demonstrated here is realized as a result of a nonequilibrium self-assembly process based on epitaxial growth with directional fluxes of Al and In under kinetically limited growth conditions. The directional fluxes promote one-axis curved nanorods curving toward the Al-rich flux side and forming an In-rich core on the opposite side. Curved nanorods grown without distinct core–shell structure with higher In content, $x \sim 0.3$, was demonstrated at lower growth temperature, 300 °C, in our previous study.²⁵ However, the crystalline quality, morphology, and compositional distribution of the nanostructures can be affected by many parameters, such as growth temperature, substrate material and orientation, magnetron power, substrate bias, working pressure, composition, incoming flux angle, and target-to-substrate distance. More work is needed to build a comprehensive knowledge of the CLEG of $\text{In}_x\text{Al}_{1-x}\text{N}$ nanostructures. On the other hand, the CLEG is a fundamentally different growth process to GLAD,^{22–24} where the growth direction mainly is governed by the directional flux and nearly negligible adatom kinetic energy. GLAD nanostructures often show an amorphous or polycrystalline microstructure with a fiber texture structure, and a broadening of rod diameter with growth time, while CLEG nanostructures are single crystals. Moreover, the CLEG nanorods are intrinsically curved, which is fundamentally different from bent nanorods.^{38,39} The latter are comprised of two distinct materials with different lattice parameters and coefficients of thermal expansions grown together side-by-side rather than a gradual composition change. Thus, bent rods have large internal strains and stresses due to the distinct lattice mismatch and unrelaxed lattices at the internal boundary between the two materials. In contrast, our CLEG curved

nanorods are expected to have negligible internal strains and stresses owing to the graded lattice constant. In addition, considering the high thermal stability of $\text{In}_x\text{Al}_{1-x}\text{N}$ thin films,^{29,30} we expect high thermal, mechanical, and structural stabilities in CLEG $\text{In}_x\text{Al}_{1-x}\text{N}$ nanostructures.

The polarizing properties of the nanostructures were examined by Mueller matrix spectroscopic ellipsometry (MMSE) using a J.A. Woollam, Co., Inc. RC2 dual rotating compensator ellipsometer.^{31,32,40} The measurements presented in this study were made in the spectral range of 245–1000 nm at an incidence angle of 25°. From the full 16-element Mueller matrix \mathbf{M} the outgoing polarization state, described with the Stokes vector $\mathbf{S}_o = [I, Q, U, V]^T$ is obtained. The degree of circular polarization $P_C = V/I$, the degree of linear polarization $P_L = ((Q^2 + U^2)^{1/2}/I)$ and total degree of polarization $P = (P_L^2 + P_C^2)^{1/2} = ((Q^2 + U^2 + V^2)^{1/2}/I)$ of the reflected light are presented.

Figure 5a shows the wavelength dependence of the degree of circular polarization P_C of light with an incident angle $\theta = 25^\circ$

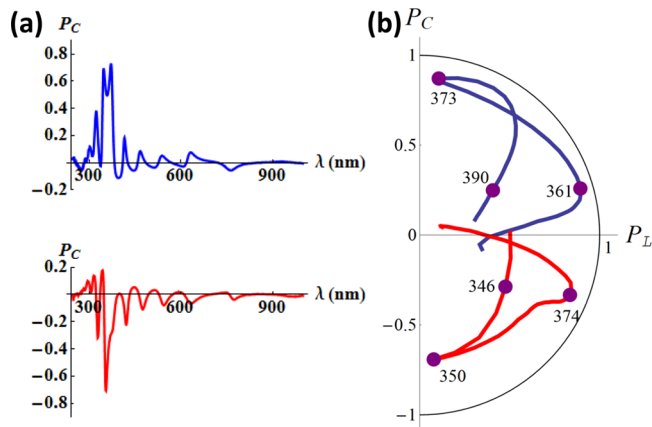


Figure 5. Degree of polarization of reflected light. (a) Wavelength dependence of degree of circular polarization (P_C) at the incident angle $\theta = 25^\circ$. The blue and red curves were obtained from right- and left-handed nanospirals, respectively. The chirality of the nanospirals gives reflections with high P_C at specific wavelengths and is dependent on the handedness of the nanospirals. (b) Polar plot showing wavelength trajectories related to P_C and degree of linear polarization (P_L). The radial distance from the origin is the total degree of polarization ($P = (P_C^2 + P_L^2)^{1/2}$).

from two nanospiral samples grown with opposite handedness but with all other parameters nominally kept the same. The data represent the case when the incoming light is unpolarized. As can be seen from the spectra, there are prominent effects on P_C with respect to both wavelength of the light and handedness of the nanospirals. The reflected light exhibits very high P_C of around ± 0.8 at 373 and 350 nm for right- and left-handed spirals, respectively, indicating nearly circular polarization. It should be pointed out that nanospiral samples with right/left handedness results in reflected light with predominantly right-/left-handed polarization. The wavelength shift of the P_C maxima between these two samples is due to slight differences in the total nanospiral height or pitch, which are important parameters governing the polarization state of the reflected light as a function of wavelength.^{7,41} More detailed optical studies and modeling have recently been presented.^{31,32}

Figure 5b shows traces in a P_C/P_L polar plot in the wavelength region of 340–400 nm for both the right- and left-

handed nanospiral sample. The total degree of polarization $P = (P_C^2 + P_L^2)^{1/2}$ is the radial distance from the origin. The wavelength trajectories for the two nanospirals are mirrored in the line $P_C = 0$. This clearly shows that the variation of both circular and linear polarization states, P_C and P_L , are highly dependent on the wavelength and exhibits opposite dependencies on chiral handedness of the nanospirals. For example, for the right-handed nanospirals the polarization of the reflected light changes from almost fully right-handed circular to almost fully linear within a wavelength range of only 12 nm while light from the other sample changes from left-handed circularly polarized to linearly polarized in a similar wavelength range. This is a distinctive behavior, which can be utilized for making polarization-tunable devices by, for example, utilizing the piezoelectric property of the wurtzite crystal structure.^{42–44}

The demonstration of tailoring of polarization state using $\text{In}_x\text{Al}_{1-x}\text{N}$ nanospirals has very important implications for potential applications in optoelectronics and electronics^{27,43} as compared to conventional oxide and fluoride nanospirals.^{12–14} Advantages of using $\text{In}_x\text{Al}_{1-x}\text{N}$ nanospirals are the tunability of optoelectronic and electrical properties combined with high thermal stability, chemical inertness, and high breakdown voltage, which enables applications in harsh environments.^{42,43} Hence, the $\text{In}_x\text{Al}_{1-x}\text{N}$ nanospirals allow operating conditions at high temperatures ($>700^\circ\text{C}$), high voltages, and high power dissipation, which is not possible for polymers and CLCs. Moreover, because modern active solid-state devices (e.g., light emitting diodes and laser diodes) for the UV-vis wavelength range are based on GaN heterostructure epitaxy, polarization controllable optoelectronic devices will be feasible by combining them with tailored isostructural $\text{In}_x\text{Al}_{1-x}\text{N}$ nanospiral coatings.

In conclusion, growth of internally laterally graded single-crystalline $\text{In}_x\text{Al}_{1-x}\text{N}$ nanospirals has been tailored with respect to handedness and pitch utilizing CLEG. Both left- and right-handed nanospirals show well-faceted hexagonal cross sections and uniform curved rod diameters without broadening throughout the whole nanospiral. The lateral compositional gradient leading to the formation of a curved lattice and morphology is confirmed by high resolution (S)TEM, EDS, and VEELS. The chirality in the nanospirals is constituted by the external spiral as well as the internally rotating anisotropic materials properties. These results in nanospiral structures which can be tailored for creating specific polarization states of light reflected off their surface. Notable is the possibility to achieve very high degree of circular polarization (P_C) with predetermined handedness. Many possibilities of using CLEG $\text{In}_x\text{Al}_{1-x}\text{N}$ -nanospirals for optical applications can be proposed. The advantages over other types of nanospirals are high P_C in the UV-vis region also for very thin layers, high stability, as well as a simple fabrication process, with high degree of controllability. This study also points toward possibilities for creating new electrical and magnetic meta materials based on tailored CLEG nanostructures, such as spirals, chevrons, and goose-necks, and also in other materials systems utilizing tailored variations of anisotropic physical properties.

ASSOCIATED CONTENT

Supporting Information

Additional figures and reference. This material is available free of charge via the Internet at <http://pubs.acs.org>.

AUTHOR INFORMATION

Corresponding Author

*E-mail: hcl@ifm.liu.se. Phone: +46-13-288928. Fax: +46-13-281704.

Author Contributions

C.-L.H., J.B., and K.J. conceived the study. C.-L.H. designed and performed the growth experiments together with P.S. and J.B. and made most of the structure characterization with interpretation. R.M and S.V. designed and performed the optical characterization together with K.J. J.P. performed the microscopy and interpreted the results together with C.-L.H., L.H., and P.O.Å.P. C.-L.H., R.M., S.V., J.B., and L.H. wrote the manuscript with revision by J.P., P.O.Å.P., and K.J. All authors analyzed and discussed the data, and agreed on the final version of the manuscript.

Notes

The authors declare no competing financial interest.

ACKNOWLEDGMENTS

This work was financially supported by Swedish Research Council (VR) under Grant 621-2012-4420, the Swedish Strategic Foundation (SSF) through the Nano-N and MS²E projects, and the Centre in Nano science and technology (CeNano) at Linköping University. The Knut and Alice Wallenberg Foundation supported our electron microscopy facility. We also want to acknowledge financial support from the Swedish Government Strategic Research Area in Materials Science on Functional Materials at Linköping University (Faculty Grant SFO-Mat-LiU 2009-00971).

REFERENCES

- (1) Parker, A. R.; Townley, H. E. *Nat. Photonics* **2007**, 2, 347–353.
- (2) Berthier, S. *Iridescences: The Physical Colors of Insects*; Springer: New York, 2006.
- (3) Sharma, V.; Crne, M.; Park, J. O.; Srinivasarao, M. *Science* **2009**, 325, 499–451.
- (4) Arwin, H.; Magnusson, R.; Landin, J.; Järrendahl, K. *Philos. Mag.* **2012**, 92, 1583–1599.
- (5) Jewell, S. A.; Vukusic, P.; Roberts, N. W. *New. J. Phys.* **2007**, 9, 99.
- (6) De Silva, L.; Hodgkinson, I.; Murray, P.; Wu, Q. H.; Arnol, M.; Leader, J.; McNaughton, A. *Electromagnetics* **2005**, 25, 391–408.
- (7) Gansel, J. K.; Thiel, M.; Rill, M. S.; Decker, M.; Bade, K.; Saile, V.; Freymann, G.; Linden, S.; Wegener, M. *Science* **2009**, 325, 1513–1515.
- (8) Zhao, Y.; Belkin, M. A.; Alù, A. *Nat. Commun.* **2012**, 3, 870.
- (9) Schäferling, M.; Dregely, D.; Hentschel, M.; Giessen, H. *Phys. Rev. X* **2012**, 2, 031010.
- (10) Liu, Y.; Zhang, X. *Chem. Soc. Rev.* **2011**, 40, 2494–2507.
- (11) Hwang, J.; Song, M. H.; Park, B.; Nishimura, S.; Toyooka, T.; Wu, J. W.; Takanishi, Y.; Ishikawa, K.; Takezoe, H. *Nat. Mater.* **2005**, 4, 383–387.
- (12) Weiglhofer, W. S.; Lakhtakia, A. *Introduction to Complex Mediums for Optics and Electromagnetics*; SPIE Press monograph: Bellingham, WA, 2003.
- (13) Hodgkinson, I.; Wu, Q. H. *Adv. Mater.* **2001**, 13, 889–897.
- (14) Young, N. O.; Kowal, J. *Nature* **1959**, 183, 104–105.
- (15) Hrudey, P. C. P.; Szeto, B.; Brett, M. J. *Appl. Phys. Lett.* **2007**, 88, 251106.
- (16) Robbie, K.; Broer, D. J.; Brett, M. J. *Nature* **1999**, 399, 764–766.
- (17) Hentschel, M.; Schäferling, M.; Weiss, T.; Liu, N.; Giessen, H. *Nano Lett.* **2012**, 12, 2542–2547.
- (18) Dolamic, I.; Knoppe, S.; Bürgi, T. *Nat. Commun.* **2012**, 3, 798.
- (19) He, Y.; Fu, J.; Zhao, Y. *Front. Phys.* **2014**, 9, 47–59.
- (20) Larsen, G. K.; He, Y.; Wang, J.; Zhao, Y. *Adv. Optical Mater.* **2014**, 2, 245–249.

- (21) Dietrich, K.; Lehr, D.; Helgert, C.; Tünnermann, A.; Kley, E.-B. *Adv. Mater.* **2012**, *24*, OP321–OP325.
- (22) Hawkeye, M. M.; Brett, M. J. *J. Vac. Sci. Technol., A* **2007**, *25*, 1317–1335.
- (23) Karabacak, T.; Singh, J. P.; Zhao, Y.-P.; Wang, G.-C.; Lu, T.-M. *Phys. Rev. B* **2003**, *68*, 125408.
- (24) Krause, K. M.; Brett, M. J. *Adv. Funct. Mater.* **2008**, *18*, 3111–3118.
- (25) Radnócz, G. Z.; Seppänen, T.; Pécz, B.; Hultman, L.; Birch, J. *Phys. Status Solidi A* **2005**, *202*, R76–R78.
- (26) Butté, R.; Carlin, J. -F.; Feltin, E.; Gonschorek, M.; Nicolay, S.; Christmann, G.; Simeonov, D.; Castiglia, A.; Dorsaz, J.; Buehlmann, H. J.; Christopoulos, S.; Baldassarri, G.; Högerthal, H. V.; A. Grundy, J. D.; Mosca, M.; Pinquier, C.; Py, M. A.; Demangeot, F. *J. Phys. D: Appl. Phys.* **2007**, *40*, 6328–6344.
- (27) Hsiao, C.-L.; Junaid, M.; Chen, R. S.; Persson, P. O. Å.; Sandström, P.; Holtz, P. O.; Hultman, L.; Birch, J. *Appl. Phys. Exp.* **2011**, *4*, 115002.
- (28) Hsiao, C.-L.; Palisaitis, J.; Junaid, M.; Persson, P. O. Å.; Jensen, J.; Zhao, Q. X.; Hultman, L.; Chen, L. C.; Chen, K. H.; Birch, J. *Thin Solid Films* **2012**, *524*, 113–120.
- (29) Seppänen, T.; Persson, P. O. Å.; Hultman, L.; Birch, J.; Radnócz, G. Z. *J. Appl. Phys.* **2005**, *97*, 083503.
- (30) Seppänen, T. *Growth and Characterization of Metastable Wide Band-gap Al_{1-x}In_xN Epilayers*. Ph.D. Thesis, Linköping Studies in Science and Technology No.1027, Linköping, 2007; ISBN: 91-85523-58-5.
- (31) Magnusson, R.; Hsiao, C.-L.; Birch, J.; Arwin, H.; Järrendahl, K. *Opt. Mater. Exp.* **2014**, *4*, 1389.
- (32) Magnusson, R.; Birch, J.; Sandström, P.; Hsiao, C. -L.; Arwin, H.; Järrendahl, K. *Thin Solid Films* **2014**, DOI: 10.1016/j.tsf.2014.02.015.
- (33) Palisaitis, J.; Hsiao, C.-L.; Hultman, L.; Birch, J.; Persson, P.O.Å. *Acta Mater.* **2013**, *61*, 4683–4688.
- (34) Palisaitis, J.; Hsiao, C.-L.; Junaid, M.; Xie, M. Y.; Darakchieva, V.; Carlin, J. F.; Grandjean, N.; Birch, J.; Hultman, L.; Persson, P. O. Å. *Phys. Status Solidi RRL* **2011**, *5*, 50–52.
- (35) Segura-Ruiz, J.; Martínez-Criado, G.; Denker, C.; Malindretos, J.; Rizzi, A. *Nano Lett.* **2014**, *6*, 1300–1305.
- (36) Cherns, D.; Webster, R. F.; Novikov, S. V.; Foxon, C. T.; Fischer, A. M.; Ponce, F. A.; Haigh, S. J. *Nanotechnology* **2014**, *25*, 215705.
- (37) Hsiao, C.-L.; Tu, L. W.; Chen, M.; Jiang, Z. W.; Fan, N. W.; Tu, Y. J.; Wang, K. R. *Jpn. J. Appl. Phys.* **2005**, *44*, L1076–L1079.
- (38) Tawfick, S.; De Volder, M.; Copic, D.; Park, S. J.; Oliver, C. R.; Polson, E. S.; Roberts, M. J.; Hart, A. J. *Adv. Mater.* **2012**, *24*, 1628–1674.
- (39) Zhang, L.; Ruh, E.; Grützmacher, D.; Dong, L.; Bell, D. J.; Nelson, B. J.; Schönenberger, C. *Nano Lett.* **2006**, *6*, 1311–1317.
- (40) Collins, R. W.; Koh, J. *J. Opt. Soc. Am. A* **1999**, *16*, 1997–2006.
- (41) Yang, Z. Y.; Zhao, M.; Lu, P. X. *IEEE Photon. Technol. Lett.* **2010**, *22*, 1303–1305.
- (42) Shimada, K.; Sota, T.; Suzuki, K. *J. Appl. Phys.* **1998**, *84*, 4951–4958.
- (43) Strite, S.; Morkoç, H. *J. Vac. Sci. Technol., B* **1992**, *10*, 1237–1266.
- (44) Su, W. S.; Chen, Y. F.; Hsiao, C.-L.; Tu, L. W. *Appl. Phys. Lett.* **2007**, *90*, 063110.